Refining the modeling strategy for anomalous electron transport in fluid simulations of Hall thrusters via insights from PIC simulations

Federico Petronio, Alejandro Alvarez Laguna, Martin Jacques Guillon, Anne Bourdon, Pascal Chabert

Refining the modeling strategy for anomalous electron transport in fluid simulations of Hall thrusters via insights from PIC simulations

Federico Petronio*,[1] Alejandro Alvarez Laguna,[1] Martin Jacques Guillon,[1] Anne Bourdon,[1] and Pascal Chabert[1]

Laboratoire de Physique des Plasmas (LPP), CNRS, Sorbonne Université, École Polytechnique, Institut Polytechnique de Paris, 91120 Palaiseau, France.

(*Electronic mail: federico.petronio@lpp.polytechnique.fr)

(Dated: 25 June 2025)

Modeling anomalous transport in fluid simulations is a fundamental challenge for developing efficient and robust fluid simulation tools for Hall thrusters. This paper investigates optimal strategies for modeling anomalous transport in such simulations. Using the particle-in-cell (PIC) benchmark (BM) setup of Charoy *et al.*, we demonstrate that the various terms in the electron momentum equation can be readily identified. In particular, we show that the assumption of expressing the rate of change of the electron momentum due to instability as proportional to the momentum itself does not hold under these simulation conditions. Subsequently, we present two fluid simulations that replicate the conditions of the PIC BM setup. The first employs the conventional empirical anomalous collision frequency approach. While this model provides generally satisfactory results, it fails to capture specific plasma characteristics. The second fluid model adopts a data-driven approach to represent the anomalous force terms in the momentum equation. This approach furnishes significantly improved results, suggesting that although the anomalous collisionality framework provides meaningful outcomes, it can be effectively replaced by more advanced techniques.

I. INTRODUCTION

Hall thrusters (HTs) have been a key technology in space propulsion for more than a half-century.[1] Despite their extensive history and widespread use, accurately simulating their behavior remains a challenging task.[2] The intrinsic complexity of plasma dynamics and interactions within the thruster necessitates the development of advanced simulation tools that can provide reliable and insightful predictions. As a result, a significant portion of current research is devoted to refining these tools and enhancing their ability to model HTs' physics with both accuracy and efficiency.

Kinetic simulations, particularly those based on Particle-in-Cell (PIC) methods[3,4], have emerged as the canonical way for capturing the intricate details of plasma behavior in HTs. These simulations provide a high level of fidelity, enabling researchers to gain detailed insights into phenomena such as plasma instabilities, wave-particle interactions, and sheath formation and dynamics. However, this precision comes at an elevated computational cost, making kinetic simulations impractical for routine use in design and optimization processes. The computational burden highlights the need for alternative methods that balance accuracy with efficiency.

Simpler stationary one-dimensional models offer an attractive alternative for exploring the fundamental physics of Hall thrusters.[5–8] By reducing the complexity of the simulation domain, these models allow for a more straightforward investigation of key phenomena and their effects on the macroscopic characteristics of the thruster. However, their stationary nature inherently limits their ability to capture the dynamic temporal behaviors of the plasma, which are critical to understanding instabilities and transient processes within the thruster. In particular, they cannot reproduce oscillations such as the breathing mode[9–11], which is a major feature of HTs. This limitation underscores the need for more versatile simulation approaches.

Unsteady fluid simulations, whether one-dimensional or two-dimensional, represent a promising middle ground between computationally intensive kinetic methods and simplified stationary models. These simulations employ fluid approximations to model plasma dynamics, enabling faster computations while retaining the capability to capture complex behaviors such as current oscillatory phenomena, i.e., the breathing mode mentioned above. The computational speed advantage is especially pronounced when employing quasi-neutral drift-diffusion models, which mitigate the large-scale separation between electron and heavy species dynamics. In contrast, more complex non-quasi-neutral models tend to be significantly more computationally demanding. The potential for fluid simulations to serve as a practical and effective tool in modeling HTs has gener-

ated significant interest, particularly for applications that require a balance between performance and computational efficiency. However, modeling complex kinetic phenomena in the fluid framework remains an important challenge.

Among these phenomena, the most relevant is the so-called anomalous transport. Several works[12–17] have shown that the electron mobility along the thruster axis, near the thruster exit and in the plume, can be 1 or 2 orders of magnitude larger than the one predicted by the classical collisional theory. Numerous possibilities have been explored about the origin of this phenomenon. The initial mechanism thought to be responsible for the enhanced mobility was the near-wall conductivity[1,12,18], related to the disruption of the closed electron Larmor orbits. However, some recent studies[19–21] proposed that this mechanism alone may be insufficient to fully explain the observed transport. Furthermore, in some HT simulations focusing on plasma-wall interactions[22–24], non-classical mechanisms—beyond near-wall conductivity—have been incorporated in some form to account for the enhanced electron cross-field transport.

Although the theory of anomalous transport driven by correlated fluctuations has been known for a long time, dating back to the work of Janes and Lowder[25], as well as the theory of the electron-cyclotron drift instability[26], it is in the past 25 years that this topic has regained significant attention within the scientific community. The pioneering work by Adam *et al.*[27] and Ducrocq *et al.*[28] identified the fluctuations of electron density and electric field as responsible for the enhanced transport in HT devices: when these fluctuations are correlated in time, a net force contributes to the electron transport in the axial direction. A decade later, Coche and Garrigues[29] validated this finding through 2D PIC simulations, while Katz *et al.*[17] introduced the concept of drag force. The work of Lafleur and colleagues[30–35] significantly advanced and corroborated the inference linking anomalous transport to azimuthal plasma instabilities.

The multi-dimensional kinetic nature of the instabilities driving the anomalous transport poses challenges for their incorporation into 1D and 2D fluid simulations. The standard approach, which is based on the work by Sagdeev and Galeev[36], involves introducing an artificial momentum-transfer collision frequency, added to the classical collisional terms. This method ensures the reproduction of observed electron transport along the thruster axis. By employing this technique, researchers and engineers have successfully used fluid and hybrid codes to replicate the macroscopic behavior of HTs[9,37–54]. However, determining the anomalous frequency value often relies on empirical considerations, and the foundational assumption by Sagdeev and Galeev remains imprecisely validated. As interestingly found by Marks and Jorns[55,56], using theoretical predictions

for the anomalous frequency directly in self-consistent simulations does not produce satisfying results. Addressing this point is crucial for advancing the reliability of HT fluid simulations and bridging the gap between theoretical predictions for anomalous transport and experimental observations.

A similar, but not equivalent, study of the collision frequency in the fluid framework was proposed by Lafleur *et al.*[57] in the context of radio-frequency discharges. In this work, the authors addressed the issue of approximating the rate of change of total electron momentum by using an effective momentum transfer collision frequency. By comparing some PIC results with usual approximations, the authors could show that conventional methods in the low-pressure plasmas community for calculating the momentum transfer collision frequency using the effective collisional frequency can be extremely inaccurate.

Direct validation of the Sagdeev and Galeev assumption is intrinsically challenging, as it is extremely difficult, if not impossible, to measure the anomalous transport contribution directly or indirectly. Furthermore, validating this theory by comparing experimental measurements with simulation outputs based on this assumption is unsatisfactory, as the simulations themselves require a predefined transport model. To address these limitations, this work focuses on analyzing PIC simulation results in which the anomalous transport contribution can be isolated from other effects. These results are then compared with fluid simulations employing different approximations for the anomalous transport term. We begin describing the theoretical model to approximate the anomalous transport in Section II. In Section III, we analyze the results of a PIC simulation configured to match the benchmark setup presented by Charoy *et al.*[58]. Sections IV and V explore two distinct fluid models: one employing the Sagdeev and Galeev assumption and the other utilizing a data-driven method to estimate the anomalous transport term. Finally, we propose a comprehensive discussion of the findings in Section VI.

II. ANOMALOUS TRANSPORT MODEL DESCRIPTION

The electron anomalous transport in HT is one of the most known and studied features of these devices. If only classical collisional transport is considered in simulations, these last fail to retrieve the macroscopic experimental evidence measured in such devices. Besides the large number of studies being performed, modeling the anomalous transport remains challenging.

Numerous studies[31–33] have shown that the best way to model the anomalous transport is to

include an anomalous force density $\mathbf{R}_{ei}$ in the electron momentum equation. Considering this force, the electron momentum equation reads

$$\frac{\partial}{\partial t}\left(m_e n_e \mathbf{v}_e\right) + \nabla \cdot \left(m_e n_e \mathbf{v}_e \mathbf{v}_e + \mathscr{P}\right) = -e n_e \mathbf{E} - e n_e \mathbf{v}_e \times \mathbf{B} - m_e n_e \nu_c \mathbf{v}_e + \mathbf{R}_{ei}, \tag{1}$$

where the electron mass is m_e, the electron density is n_e, the electron velocity is $\mathbf{v}_e$, the electron pressure tensor is $\mathscr{P}$, the electron charge is $-e$, the electric field vector is $\mathbf{E}$, the magnetic field vector is $\mathbf{B}$, the electron classical collision frequency is ν_c.

The usual approach, based on a work from Sagdeev and Galeev[36], consists of approximating the rate of change of momentum along the direction j as

$$R^j_{ei} \sim \frac{\delta}{\delta t}\left[m_e n_e v_{e,j}\right]_{ei} = -m_e n_e v_{e,j} \nu_a. \tag{2}$$

In the previous expression, we introduced the anomalous frequency ν_a. If the anomalous frequency has the same value in all directions, the electron momentum equation can be rewritten as

$$\frac{\partial}{\partial t}\left(m_e n_e \mathbf{v}_e\right) + \frac{\partial}{\partial x}\left(m_e n_e \mathbf{v}_e \mathbf{v}_e + \mathscr{P}\right) = -e n_e \mathbf{E} - e n_e \mathbf{v}_e \times \mathbf{B} - m_e n_e (\nu_c + \nu_a) \mathbf{v}_e. \tag{3}$$

The collision frequency ν_c is used in some cases to calculate the heat flux closure by Fourier's law[59]. However, using the total collision frequency, including the anomalous collision frequency (i.e. $\nu_c + \nu_a$), for particle diffusion in the heat flux calculation, may give a good order of magnitude for the heat flux, but would require more precise justification.

As noted in the introduction, the approach described in this section has been effectively applied in 1D fluid as well as 2D hybrid and fluid simulations, showing good agreement with experimental data[42,46,48,60]. Nevertheless, these fluid models inherently assume the validity of the Sagdeev and Galeev hypothesis, and use for the electron momentum equation an expression similar to the one in Eq. (3). We believe that gaining deeper insights into the truth of this hypothesis is crucial for improving the modeling of anomalous transport.

III. PIC RESULTS

The simulation setup is inspired by the 2D PIC simulation as defined by Boeuf and Garrigues[61] and later used by Charoy *et al.*[58] in their well-known benchmark paper. We selected this simulation configuration for some main reasons: i) its renowned setup, ii) its simplicity, and iii) the fact that a quasi-steady state is reached. This last characteristic allows us to estimate the stationary components of the momentum equation and to analyze them precisely.

Anomalous frequency study

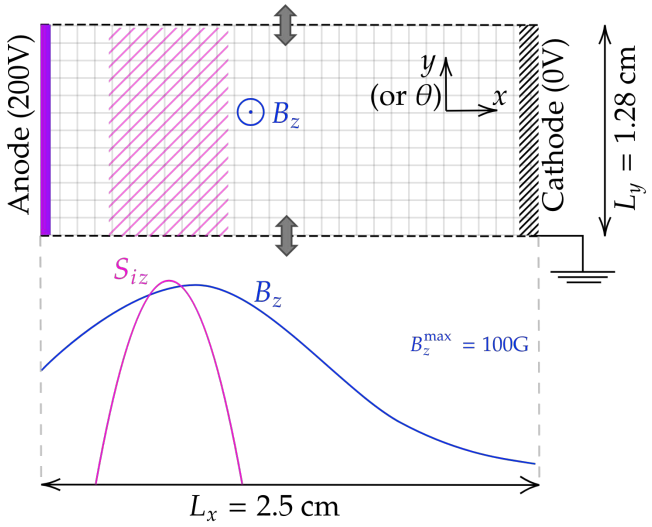

FIG. 1: The simulation domain used in the Charoy *et al.*[58] benchmark testcase. The ionization is imposed in the magenta area. The magnetic field peaks at $x = 0.75$ cm is out-of-plane and constant in time. The anode (at the left) is at a constant high voltage, while the cathode (at the right) is grounded.

A. PIC simulation setup

Figure 1 presents the two-dimensional Cartesian simulation domain (with periodic boundaries in the azimuthal direction), along with the imposed magnetic and ionization profiles. The domain is a rectangular box, measuring $L_x = 2.5$ cm in the axial (thrust) direction and $L_y = 1.28$ cm in the azimuthal direction.

Particles crossing the left or right boundaries of the domain are removed from the simulation. To maintain current continuity and ensure charge neutralization of the extracted ion beam, electrons are injected from a cathode plane positioned 1 mm inside the right boundary of the domain. The number of electrons injected at each time step is determined to preserve current balance across the discharge. Specifically, by tracking the number of electrons and ions crossing the anode boundary at each time step (denoted as ΔN_{ea} and ΔN_{ia}, respectively), the corresponding number of electrons to be emitted from the cathode plane is set to $\Delta N_{ea} - \Delta N_{ia}$.

In this simulation, the ionization profile is imposed, and the dynamics of neutral particles is

not modeled. Consequently, collisions between charged particles and neutrals are neglected, and collisional electron transport is not included. At each time step, an equal number of electrons and xenon ions are injected following a parabolic ionization profile. This corresponds to a current density of $J_M = 400\,\mathrm{A/m^2}$. The anode, located at the left boundary, is held at a constant high voltage.

The magnetic field is constant in time, oriented out of the simulation plane, and azimuthally invariant. Its axial Gaussian profile is shown at the bottom of Figure 1. It is worth noting that since plasma–wall interactions in the out-of-plane direction are not modeled, no information regarding thruster wall geometry is required for this configuration.

The simulation is run for 10 µs, once quasi-steady state has been reached, which typically occurs after approximately 10 to 15 µs. Additional details regarding the PIC simulation setup are provided in the Appendix. The complete implementation specifications follow those described in the benchmark study by Charoy *et al.*[58].

The code used to generate the results is LPPic, of which all characteristics are given in the benchmark papers[58,62]. The more recent works[11,63] also include the late developments. Some analysis of the results of an equivalent simulation can also be found in ref.[64]

B. Analysis of the PIC simulation results

By analyzing the electron momentum conservation equation, we can try to directly estimate the validity of the expression proposed by Sagdeev and Galeev in Eq. (2). Intending to understand the contribution of the different terms of the momentum equation, we analyze each component of this equation, as proposed by Lafleur and Chabert[32]. In Figure 2, the axial profiles of the different terms of the electron momentum equation along the thruster axis x show the only four terms of the electron momentum equation that are not negligible. A detailed study of these terms in the BM test case, along with an analysis of the possible models for the anomalous force term, has been published by Charoy *et al.*[64]. The friction force term (e.g. R_{ei} in Eq. (1)) is estimated along direction j by calculating the correlation term[30],

$$R_{ei}^{j} = e\langle \delta E_j \delta n_e \rangle = e\langle [\langle n_e \rangle_t - n_e(t)][\langle E_j \rangle_t - E_j(t)] \rangle_t. \tag{4}$$

The angle brackets $\langle\rangle_t$ represent a time average over a defined time interval.

Figure 2 (a) demonstrates that the electron momentum equation along the azimuthal (i.e. y) direction can be successfully decomposed in four major terms: the magnetic force density (i.e.

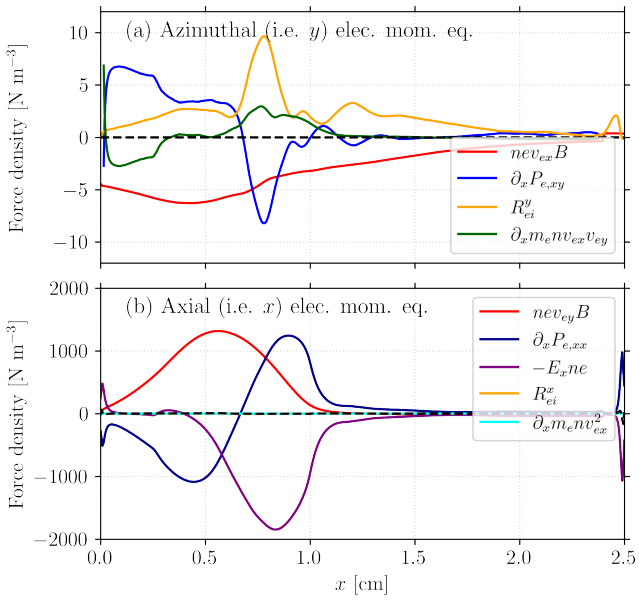

FIG. 2: The dominating terms of the electron momentum equation extracted from PIC along azimuthal (a) and axial (b) directions.

$n_e e v_{ex} B$), the instability-enhanced friction force density (i.e. R^y_{ei}), the azimuthal spatial inertia (i.e. $\partial_x m_e n_e v_{ex} v_{ey}$), and the off-diagonal pressure tensor gradient (i.e. $\partial_x P_{e,xy}$). The term ∂_x denotes the spatial derivative along the thruster axis direction. Each of these quantities is the result of a temporal and azimuthal average of the quasi-steady state PIC results. The friction force is obtained by averaging over time intervals of 0.375 µs. We highlight that the sum of the various terms equating to zero indicates that the anomalous force density term can be directly computed from the PIC data.

In the same way, Figure 2 (b) shows that the electron momentum equation along the axial direction is dominated by the electric force (i.e. $-E_x n_e e$), the magnetic force (i.e. $n_e e v_{ey} B$), and the pressure gradient (i.e. $\partial_x P_{e,xx} = \partial_x n_e e T_{e,xx}$, with the electron temperature $T_{e,xx}$ expressed in eV). The anomalous force density along the axial direction, $R^x_{ei} = e\langle \delta E_x \delta n_e \rangle$, is negligible when compared to the aforementioned terms. However, we underline the fact that R^x_{ei} and R^y_{ei} have the same order of magnitude, per se. It is then relevant to evaluate the anomalous collision frequency also along the axial direction, since in the usual approach in Eq. (3) an anomalous frequency is

Anomalous frequency study

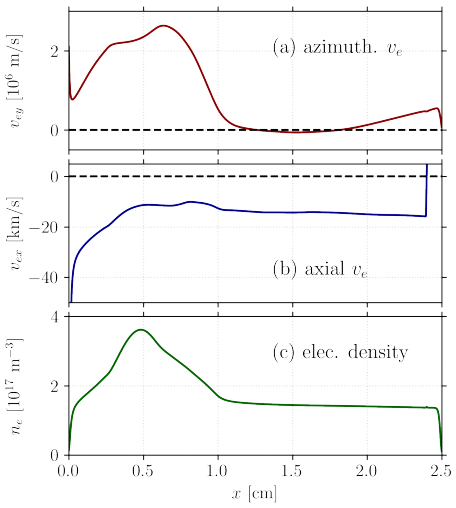

FIG. 3: Axial profiles extracted from the PIC simulation of the azimuthal electron velocity (a), the axial electron velocity (b), and the plasma density (c). The sharp increment of $v_{e,x}$ near the left boundary is an artifact related to the presence of the cathode and should be disregarded.

used also in the momentum equation along this direction.

By calculating the electron axial profiles of velocities and density (cf. Figure 3), and the anomalous force profiles, one can estimate a value of the effective anomalous collision frequency $\nu_a^{x,y}$ for x and y directions by the expression in Eq. (2), as

$$\nu_a^{x,y} = -\frac{R_{ei}^{x,y}}{m_e v_{e,x,y} n_e}.$$

In the literature, it is common to express the anomalous parameter of this Bohm-type electron diffusion by dividing the actual frequency by the electron cyclotron frequency ω_{ce}:

$$\alpha_B^{x,y} = \frac{\nu_a^{x,y}}{\omega_{ce}} = -\frac{R_{ei}^{x,y}}{eBv_{e,x,y} n_e}.$$

One should notice that the electron azimuthal velocity in Figure 3 (a) is close to zero or even negative in the region between $x \approx 1.3$ cm and $x \approx 1.7$ cm. This is related to the strong axial pressure gradient, generating a diamagnetic drift opposite to the well-known $\mathbf{E} \times \mathbf{B}$ drift. A complete discussion of this phenomenon in an equivalent simulation setup is given by Boeuf and Garrigues[61].

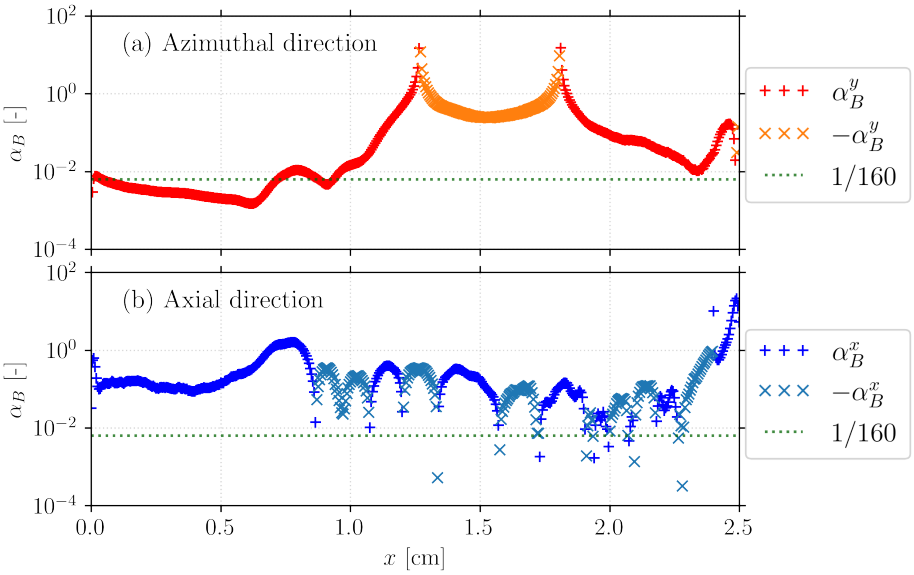

FIG. 4: Estimation of the anomalous frequency coefficient $\alpha_B = \nu_a/\omega_{ce}$ in azimuthal (a) and axial (b) directions, as estimated from PIC. The minus sign allows us to plot also the negative values of α_B. The dotted line represents $\alpha_B = 1/160$, which is a usual value used in simulations[40].

In Figure 4 (a) and (b), we report the values of $\alpha_B^{x,y}$ calculated along the azimuthal and axial directions, respectively. These values are computed at quasi-steady state at t =20 µs. We confirmed that the terms of the electron momentum equation exhibit no significant variation throughout the quasi-steady simulation's span. Therefore, any individual time point, or the time-averaged state, can be reliably used to determine the value of α_B. For reference, we also include in Figure 4 an empirical value for this coefficient, namely $\alpha_B = 1/160$, which is of the same order of magnitude as those typically used in simulations[40,41,51]. As one can notice in this figure, the values of α_B^x and α_B^y are far from constant. Moreover, we observe several sign variations there.

In the azimuthal direction, i.e., Figure 4 (a), within the thruster channel, the value of α_B^y is relatively constant and close to the empirical value. On the contrary, in the thruster plume, the value of α_B^y estimated from PIC is significantly larger (in absolute value) than the empirical one. This fact is related to the small absolute value of the azimuthal electron velocity, cf. Figure 3 (a). In the same figure, we observe that we have a sign-change of the velocity, which makes the value

of α_B^y, so the anomalous frequency, negative. This would lead to several physical inconsistencies.

The results are not better when we try to calculate α_B^x in Figure 4 (b). Along this direction, the friction force plays only a minor role, as shown by Charoy *et al.*[64], its value is orders of magnitude lower than other axial electron momentum equation terms. In particular, a large number of sign-variations of R_{ei}^x in the thruster plume make it very difficult to obtain an estimation of the value of α_B from these data.

All in all, this approach is not very satisfying. The PIC results show that it is possible to calculate precisely the anomalous transport contribution to the electron momentum equation, but, when trying to derive an anomalous frequency from it, the model from Sagdeev and Galeev[36] fails to produce an exploitable anomalous frequency. In this case, the anomalous force cannot be expressed as the product of a frequency and the electrons' momentum. Specifically, the changes in the sign of the azimuthal velocity result in an anomalous collision frequency varying in sign, a behavior that does not appear to be physically meaningful. Moreover, using the same anomalous frequency along the two directions does not appear justified either. Nevertheless, it is interesting to verify whether or not sensible results can be obtained from fluid simulations employing the anomalous frequency.

IV. FLUID MODEL WITH ANOMALOUS COLLISION FREQUENCY

In Section III B, we have shown that there is no straightforward way to derive the anomalous collision frequency from PIC results. It is crucial to thoroughly understand the potential limitations and significant advantages associated with the use of anomalous frequency. Therefore, in this section, after following the conventional empirical approach to derive the anomalous frequency, we present some results obtained with this approximation.

1. Description of the fluid model with anomalous frequency

We consider a quasi-neutral plasma with density n, without a background gas, in a 1D domain. The parameters of the simulation correspond to those of the PIC, averaged azimuthally. We consider a simulation length of $L = 2.5\,\text{cm}$ with the out-of-plane magnetic field and ionization source described in Section III A. We highlight that in these simulation conditions, the electrons are magnetized and their motion is significant in both axial and azimuthal directions. On the contrary, the

ions are not magnetized, and we can safely limit our study to their motion in the axial direction. The fluid system of equations is composed of four equations, which read

$$\frac{\partial n}{\partial t}+\frac{\partial (v_i n)}{\partial x}=S_{iz}, \quad \text{Ion continuity equation}$$
$$\frac{\partial (Mnv_i)}{\partial t}+\frac{\partial \left(Mnv_i^2\right)}{\partial x}=enE_x+m_e n v_{e,x}\nu_a, \quad \text{Momentum equation for ions}$$
$$\frac{\partial m_e n v_{e,y}}{\partial t}+\frac{\partial m_e n v_{e,y}v_{e,x}}{\partial x}=-m_e n v_{e,y}\nu_a+env_{e,x}B, \quad \text{Azim. momentum for electrons}$$
$$\frac{\partial}{\partial t}\left(\frac{3}{2}neT_e+\frac{1}{2}m_e n v_{ey}^2\right)+\frac{\partial}{\partial x}\left(\frac{5}{2}neT_e v_{ex}+\frac{1}{2}m_e n v_{ey}^2 v_{ex}\right)=$$
$$=-nev_{ex}E_x+\frac{3}{2}eT_e^{inj}S_{iz}. \quad \text{Energy equation for electrons}$$

In the previous set of equations, we explicitly write the anomalous terms in the axial momentum equations for ions and in the azimuthal momentum equation for electrons. The xenon ion mass is indicated by M. The system is closed by an isotropic closure for the temperature T_e, expressed in eV, and by considering a stationary axial electron momentum equation:

$$enE_x=-\frac{\partial \left(neT_e\right)}{\partial x}-env_{ey}B-m_e n v_{e,x}\nu_a.$$

The total current density defined as

$$J_0=en(v_{i,x}-v_{e,x}),$$

can be retrieved by integrating the stationary electron momentum equation, and reads

$$J_0=\frac{V_0+\int_0^{L_x}\left(v_{e,y}B+\frac{m_e v_{i,x}\nu_a}{e}+\frac{\partial_x\left(neT_e\right)}{en}\right)dx}{\int_0^{L_x}\frac{m_e\nu_a}{en}dx}. \tag{5}$$

In the previous expression, L_x is the length between the high-voltage anode, kept at potential V_0, and the grounded cathode. Equation (5), similar to the one used in Ref.[51], is added to the set of differential equations. We have further imposed the following conditions on the left boundary:

$$v_i(x=0)=-\sqrt{\frac{eT_e(x=0)}{M}},$$

and on the right boundary for the temperature:

$$T_e(x=L_x)=10\,\text{eV},$$

and for the electron azimuthal speed:

$$v_{e,y}(x = L_x) = 0.$$

As the ion flow is supersonic at the right boundary, it is not possible to impose a boundary condition at that location for the ion velocity. The ion Bohm velocity imposed at the left boundary is associated with a voltage drop across the plasma sheath near the anode wall[5]. This voltage drop is relatively small (e.g., from PIC we expect it to be around 6% of the total voltage drop across the discharge). For this reason, it has been neglected in the present simulations. While more advanced fluid models could incorporate this effect, such an extension lies beyond the scope of the current study.

It is, however, important to highlight that the original PIC test case designed by Boeuf and Garrigues[61] was intended to investigate only the ionization and acceleration regions of a HT. It does not simulate the full channel length, but rather only the external $\sim 75\,\mathrm{mm}$ of a standard HT channel. As a result, the temperature peak lies critically close to the left boundary of the simulation domain.

Although the off-diagonal pressure term appears significant in Figure 2, we have not included it here, consistent with standard practice in the literature[40], as no simple closure is currently available. Moreover, in a full kinetic theory framework, an anomalous energy transport term is also expected, possibly characterized by a different anomalous collision frequency or structure[33]. However, this term is not considered here. The numerical details of the resolution are given in the Appendix.

In order to identify the values of $\nu_a = \alpha_B \omega_{ce}$, we used an iterative approach adjusting the value of α_B to match the total current. We know that other choices can be made; however, the matching of the current remains one of the most commonly used. We used for α_B a two values-model, selecting a value α_B^{ch} for the channel $x < 0.725\,\mathrm{cm}$ and α_B^{pl} for the plume $x > 0.775\,\mathrm{cm}$. In a region of $0.05\,\mathrm{cm}$, centered in $x = 0.75\,\mathrm{cm}$, the anomalous frequency coefficient is varied linearly between α_B^{ch} and α_B^{pl}. After filling in a 2D map reported in Figure 5, we selected the pairs $(\alpha_B^{\mathrm{ch}}, \alpha_B^{\mathrm{pl}})$ on the $J \approx 690\,\mathrm{A\,m^{-2}}$ level line. We highlight that a rather broad variety of values of α_B^{ch} allows us to obtain the desired current value, while the value of α_B^{pl} is limited between ~ 0.020 and ~ 0.025.

To select the desired values, we have a supplementary degree of freedom. Figure 6 illustrates how the plasma parameters vary along the thruster axis as different values of $(\alpha_B^{\mathrm{ch}}, \alpha_B^{\mathrm{pl}})$ are selected. It is worth noting that in our implementation, variations in α_B have a minor effect on the

Anomalous frequency study

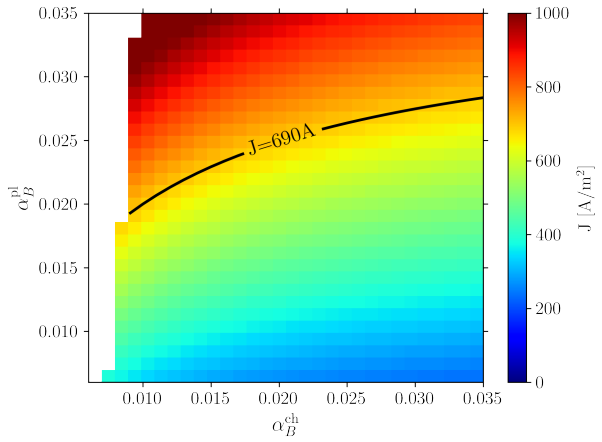

FIG. 5: Variation of the current density as a function of the anomalous transport parameters. In the white area on the left, the simulation did not converge.

axial ion velocity and plasma density at the right boundary, and thus on the overall thrust. The most significantly affected quantities are the axial and azimuthal electron velocities, with a minor impact also observed on the plasma density. Our choice of the pair $(\alpha_B^{\mathrm{ch}}, \alpha_B^{\mathrm{pl}})$ has been a trade-off between the different parameters: we eventually selected the case that best matches the maximal density. However, if we had made a different choice on the $J = 690\,\mathrm{Am}^{-2}$ level line, the results would not have been substantially different.

The values of α_B selected for this study are

$$\begin{cases} \alpha_B^{\mathrm{ch}} &= 0.016, \\ \alpha_B^{\mathrm{pl}} &= 0.024. \end{cases}$$

These parameter values allow us to reproduce the overall current density from the fluid simulation with an accuracy within 5% when compared to the corresponding PIC simulation. To make the analysis as clear as possible, we will keep these values fixed for the rest of this section and set them as the default ones. In Section V B, we will also consider a different pair, i.e., $(\alpha_B^{\mathrm{ch}} = 0.008, \alpha_B^{\mathrm{pl}} = 0.018)$, selected to better match the electron and ion current density profiles.

We highlight that these values of α_B are slightly larger than the ones normally used in this framework, which are usually around $\alpha_B = 1/160$[40].

Anomalous frequency study

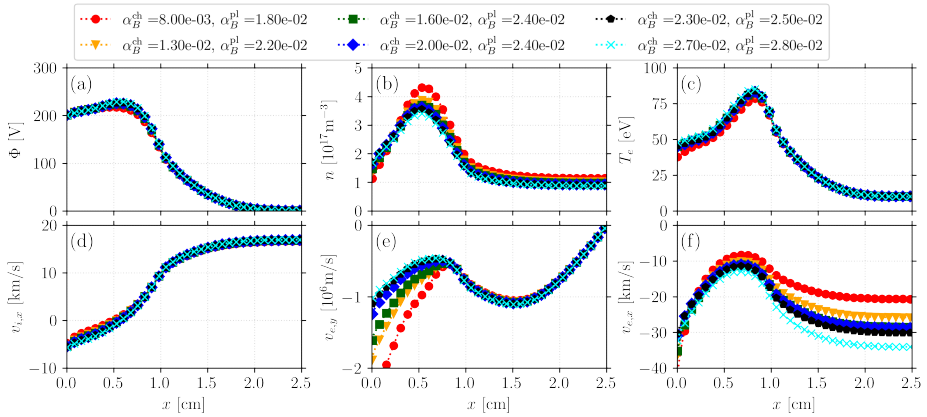

FIG. 6: Axial profiles of potential (a), plasma density (b), plasma temperature (c), axial ion velocity (d), azimuthal electron velocity (e), and axial electron velocity (f) for different pairs $(\alpha_B^{ch}, \alpha_B^{pl})$, as reported in the legend.

2. *Results of the fluid simulation using anomalous frequency*

To discuss the validity of the assumptions discussed in Section IV, the results of such fluid simulation should be compared with the results obtained from the PIC simulations. In Figure 7 we show the comparison of the profiles along the thruster axis of several plasma parameters from fluid and PIC simulations.

The results in Figure 7 are overall satisfying. The figure shows that the fluid model successfully renders the major plasma characteristics extracted from PIC results. The shape of the plasma potential produced by the fluid code is similar to the PIC one, even if we notice a less steep drop in the potential. The plasma density is very well reproduced, even though we slightly underestimated the density in the plasma plume. The electron temperature is largely overestimated, likely due to the lack of heat flux modeling, but the typical bell shape of the temperature profile is still well captured. We observe that the fluid model well replicates the ion velocity: the difference between PIC and fluid is visible, but small.

When we come to the electron velocity, the situation changes. The electron axial velocity, cf. subfigure (f), is satisfactorily rendered by the fluid model in the anode region. The other way around, the electron axial velocity in the plume calculated by the fluid code is largely overesti-

Anomalous frequency study

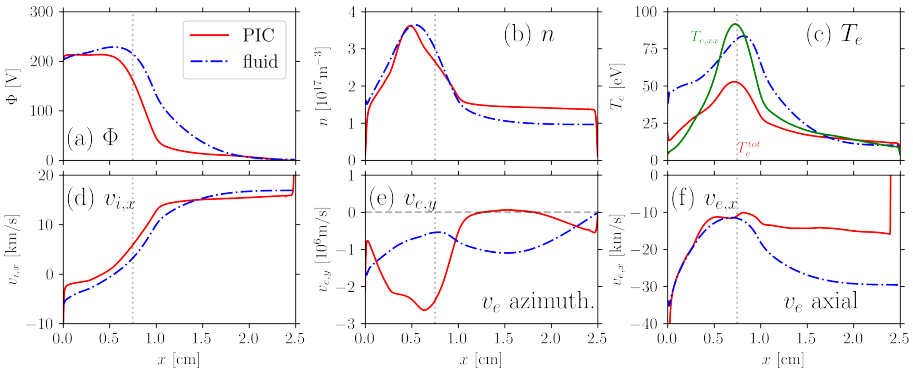

FIG. 7: Axial profiles of fluid (dashed blue) and PIC (red) results for potential (a), plasma density (b), plasma temperature (c), axial ion velocity (d), azimuthal electron velocity (e), and axial electron velocity (f). The vertical dotted line corresponds to the magnetic field maximum. PIC results are azimuthally averaged. The fluid model uses an anomalous frequency with $(\alpha_B^{\mathrm{ch}} = 0.016,\ \alpha_B^{\mathrm{pl}} = 0.024)$.

mated: its absolute value is twice as large in the fluid as in PIC. This becomes even worse when we look at the azimuthal electron velocity, cf. subfigure (e). Even though the code produces good orders of magnitude for this velocity, the axial profile produced from the fluid code is not at all similar to the one obtained from PIC.

3. *Analysis of the electron momentum equation*

In order to understand the differences between the fluid and PIC results, we analyze the electron momentum equation. In Figure 8, we show the axial profiles of the different terms of the electron momentum equation along the thruster axis x, explicitly comparing PIC and fluid results. By looking at subfigures 8 (a) and (b), we can see that PIC and fluid simulations produce very similar results. Even if some variations persist, the dominating terms are the same in both simulations. Among them, the largest difference is related to the wrong azimuthal electron speed in the fluid simulation, which is responsible for the difference in the magnetic force density (yellow line).

The similar profiles obtained along the axial directions are not confirmed when we look at the azimuthal momentum equation, cf. Figure 9. In this figure, we show the azimuthal profiles of

Anomalous frequency study

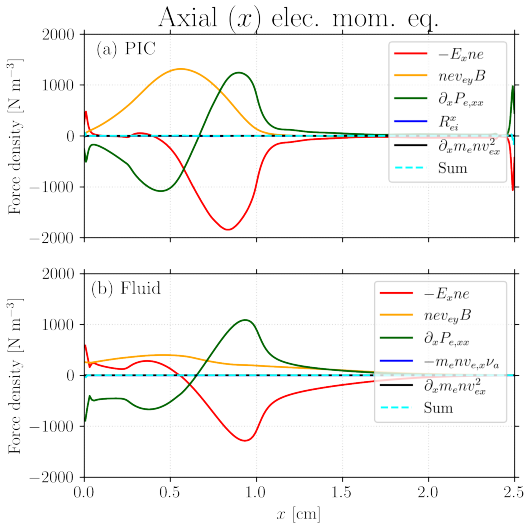

FIG. 8: Axial profiles of the electron axial momentum equation terms from PIC (a), and fluid (b) simulations.

the different terms of the electron momentum equation along y, averaged azimuthally. As one can notice by looking at the red line in Figure 9, the magnetic force density in the axial direction is well modeled by the fluid approximation. This is not the case for the anomalous force, the off-diagonal spatial inertia term $m_e n v_{ex} v_{ey}$, and the pressure gradient term $\partial_x P_{e,xy}$. In the fluid simulation, the off-diagonal inertia term is significantly underestimated, while the anomalous force density has a good order of magnitude, but a noticeably different profile.

By summing the different terms of the electron momentum equation from the PIC aforementioned and comparing them to the fluid, cf. Figure 10, we can study the effect of the anomalous force introduced in this way. As one can see, in the fluid model, the anomalous force density term is the counterpart of the combined effect of the real anomalous force, the off-diagonal spatial inertia term, and the off-diagonal inertia term.

Anomalous frequency study

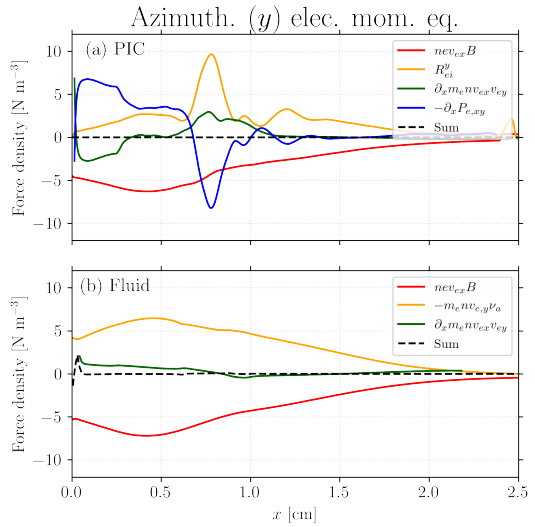

FIG. 9: Axial profiles of the electron azimuthal momentum equation terms from PIC (a), and fluid (b) simulations.

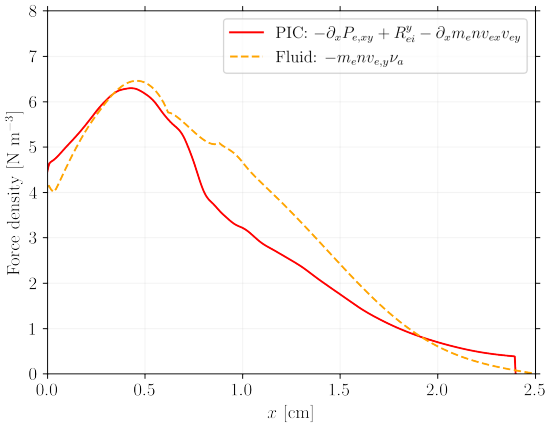

FIG. 10: Comparison of a selection of the azimuthal electron momentum equation terms from PIC (red) and fluid (yellow) simulations.

V. FLUID MODEL WITH DATA-DRIVEN ANOMALOUS FORCE

The results in Section IV show that it is possible to obtain a reasonably good comparison between the fluid and the PIC results by introducing an anomalous force density in the momentum equation, proportional to an empirical anomalous frequency. However, as explained in Section III B, the theoretical justifications for considering such an anomalous force model are, in the present simulation setup, weak.

Although theoretical closures for the anomalous force term appear to be the most attractive approach, we propose an intermediate method here. Specifically, we present an alternative empirical model that incorporates certain terms, derived from PIC results, directly into the fluid model instead of relying on the anomalous frequency framework.

A. Description of the fluid model using data-driven anomalous force

The fluid system of equations is based on the one discussed in Section IV, with some differences, and reads

$$\frac{\partial n}{\partial t}+\frac{\partial (v_i n)}{\partial x}=S_{iz}, \quad \text{Ion continuity equation}$$

$$\frac{\partial (Mnv_i)}{\partial t}+\frac{\partial \left(Mnv_i^2\right)}{\partial x}=enE_x+R_{ie}^x, \quad \text{Momentum equation for ions}$$

$$\frac{\partial m_e n v_{e,y}}{\partial t}+\frac{\partial \left(m_e n v_{e,y} v_{e,x}+P_{e,xy}\right)}{\partial x}=R_{ei}^y+env_{e,x}B, \quad \text{Azim. momentum for electrons}$$

$$\frac{\partial}{\partial t}\left(\frac{3}{2}neT_e+\frac{1}{2}m_e n v_{ey}^2\right)+\frac{\partial}{\partial x}\left(\frac{5}{2}neT_e v_{ex}+\frac{1}{2}m_e n v_{ey}^2 v_{ex}+P_{e,xy}v_{ey}\right)=$$

$$=-nev_{ex}E_x+\frac{3}{2}eT_e^{inj}S_{iz}. \quad \text{Energy equation for electrons}$$

The reader can notice that we directly introduce in the model the anomalous force density terms directly extracted from PIC (i.e. R_{ie}^x and R_{ei}^y), as well as the off-diagonal pressure gradient term $P_{e,xy}$. The term R_{ie}^x in the ion momentum equation models the effect of the anomalous force on the ions' momentum and it is such $R_{ie}^x=-R_{ei}^x$. We use again an isotropic closure for the temperature and the axial electron momentum equation

$$enE_x=-\frac{\partial neT_e}{\partial x}-env_{ey}B+R_{ei}^x.$$

The values of R_{ei}^x, R_{ei}^y, and $P_{e,xy}$ are constant in time, given that the simulation converges toward a quasi-steady state, and are provided directly as input, as they are extracted from PIC. In the energy

equation, we neglected the heat flux, as a theoretical closure (e.g., Fourier's law) could not be applied due to the absence of a well-defined thermal conductivity, and a data-driven closure did not produce satisfactory results. The data-driven heat flux exhibited significant temporal variations in the PIC simulation, making it uncertain to depend on an average value. Further research is necessary to address this issue.

One should notice that the numerical scheme requires adaptation. In particular, when computing the current density. The current, necessary to impose the voltage boundary conditions, is calculated here as

$$J_0 = \frac{V_0 + \int_0^{L_x} \left(\frac{\partial_x n e T_e}{en} + v_{ey} B + \frac{(R_{ei}^x - R_{ei}^y)}{en} + v_{ix} B - \frac{\partial_t (m_e n v_{ey})}{en} - \frac{\partial_x (m_e n v_{ey} v_{ex})}{en} \right) dx}{\int_0^{L_x} \left(\frac{B}{n} - \frac{m}{en} \partial_x v_{ey} \right) dx}.$$

The time derivative of the azimuthal electron momentum can be neglected. This is reasonable in the case of a quasi-steady state such as the one reached in the current setup. As before, the current density equation is added to the set of differential equations. All in all, the fluid model is solved using a standard approach, where R_{ei}^x, R_{ei}^y, and $P_{e,xy}$ are computed by azimuthally averaging the PIC outputs and then supplied as tabulated inputs to the fluid code.

B. Results of the fluid model using data-driven anomalous force

The results of this second fluid model are reported in Figure 11, which is the counterpart for the data-driven fluid model of Figure 7, which reported the results of the first. In subfigure (a), the electric potential from the fluid simulation is again very close to the one obtained from PIC. These results are slightly better than before. For what concerns the density, the maximal density in the channel is now underestimated with respect to the fluid PIC one. On the contrary, the density in the plume from the data-driven fluid simulation is extremely close to the one from PIC.

The electron temperature is still largely overestimated, but the shape of the temperature profile is again nicely rendered. We highlight that the temperature estimation becomes extremely accurate in the plume, for $x > 1\,\mathrm{cm}$, which was not the case for the previous fluid model. The ion velocity is also satisfactorily reproduced, with a small difference in the plume, where the velocity is underestimated.

The electron velocity is the parameter that is affected the most by introducing the data-driven anomalous force density. The most remarkable result is that with the present model, the electron

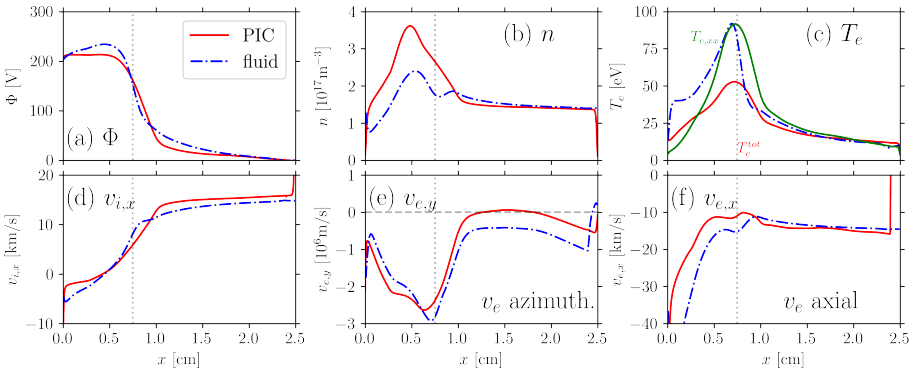

FIG. 11: Axial profiles of fluid (dashed blue) and PIC (red) results for potential (a), plasma density (b), plasma temperature (c), axial ion velocity (d), azimuthal electron velocity (e), and axial electron velocity (f). The vertical dotted line corresponds to the magnetic field maximum. PIC results are azimuthally averaged. The fluid model uses a data-driven anomalous force.

velocity in the azimuthal direction is extremely close to the one calculated from the PIC simulation. If we compare the azimuthal velocity profile in Figure 11 (e), with the results previously obtained with the anomalous frequency model, cf. Figure 7 (e), we see how the estimation of this parameter has improved. The axial electron velocity is also well represented. In particular, we notice that the estimation of the electron velocity in the plume is now much better than with the previous model. However, in the anode region ($x < 0.75\,$cm), the absolute value of the electron velocity is now overestimated, which is consistent with the underestimated electron density in this region. The origin of this phenomenon is still unclear; however, it is probably related to a lack in the modeling of the energy transport. In the fluid model, tuning the anomalous transport coefficient effectively results in an indirect adjustment of the electron axial velocity. As a consequence, it is not surprising that the axial electron velocity closely matches the one observed in the PIC simulation. In contrast, the data-driven model lacks an explicit treatment of energy transport, leading to an overestimation of the electron temperature. This elevated temperature is compensated by a lower plasma density, which in turn results in an increased axial electron velocity.

Contrary to the approach where we adjusted the anomalous collision frequency to match the overall current density, in the model employing the data-driven anomalous force, the total current is not imposed but rather obtained as the sum of the electron and ion components. As shown

Anomalous frequency study

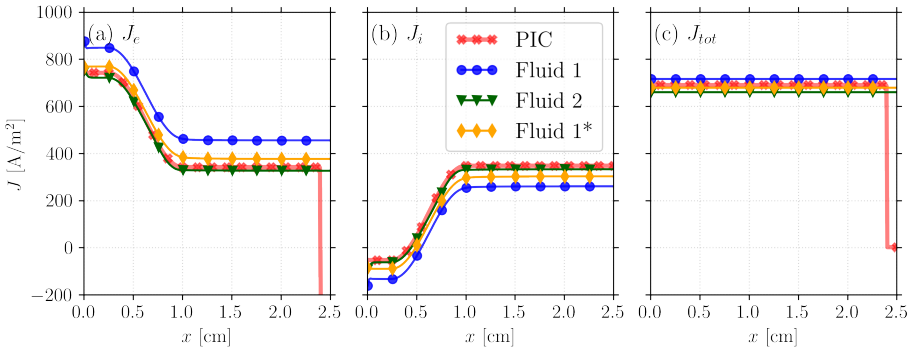

FIG. 12: Current density components: electrons (a), ions (b), and total (c). In red we show the PIC results, in blue the results for the model using the anomalous frequency (i.e., Fluid 1 in the legend, with $(\alpha_B^{\text{ch}} = 0.016, \alpha_B^{\text{pl}} = 0.024)$), and in green the results for the model using the data-driven anomalous force (i.e., Fluid 2 in the legend). The orange line (i.e., Fluid 1* in the legend) shows the results obtained using $(\alpha_B^{\text{ch}} = 0.008, \alpha_B^{\text{pl}} = 0.018)$ in the first fluid model.

in Figure 12 (c), the total current density predicted by the data-driven model remains within 5% of the PIC total current, specifically exhibiting a deviation of 4.5% below the PIC reference. In this figure, the PIC results are depicted in red, while the results for the model using the anomalous frequency (Fluid 1 in the legend) are shown in blue, and those for the model employing the data-driven anomalous force (Fluid 2 in the legend) are represented in green. As mentioned in Section III B, the discontinuity near the right boundary in PIC results is due to the cathode emission model and should be considered an artifact.

A more detailed analysis of each current component is presented in subfigures (a) and (b), corresponding to electrons and ions, respectively. Notably, the data-driven anomalous force model accurately captures the current density profiles along the thruster axis for both electrons and ions. In contrast, while the anomalous frequency model ensures the correct total current—since it is explicitly tuned to match this quantity—it exhibits a significant deviation in the individual electron and ion current components compared to the PIC results.

Consistent with the analysis presented in Figure 6, we also report in Figure 12 the results obtained using an alternative set of α_B values, specifically $(\alpha_B^{\text{ch}} = 0.008,\ \alpha_B^{\text{pl}} = 0.018)$, which were selected to better match the current density profiles of the species. This choice of parameters leads to an improved estimation of both electron and ion current densities. Nonetheless, the accuracy

Anomalous frequency study

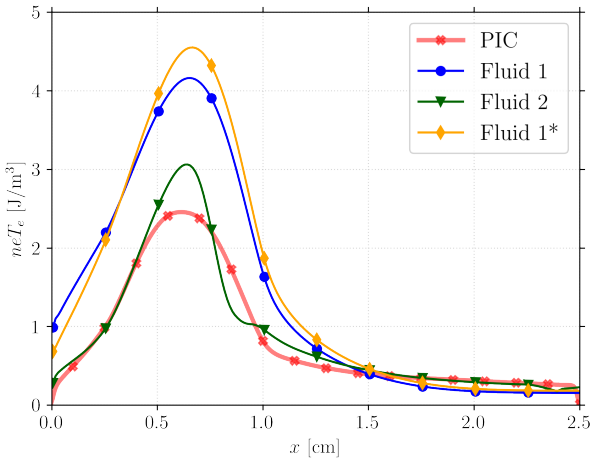

FIG. 13: Electron pressure neT_e, in blue the results for the model using the anomalous frequency (i.e., Fluid 1 in the legend, with $(\alpha_B^{\text{ch}} = 0.016, \alpha_B^{\text{pl}} = 0.024)$), and in green the results for the model using the data-driven anomalous force (i.e., Fluid 2 in the legend). The orange line (i.e., Fluid 1* in the legend) shows the results obtained using $(\alpha_B^{\text{ch}} = 0.008, \alpha_B^{\text{pl}} = 0.018)$ in the first fluid model.

achieved with the data-driven (i.e., Fluid 2 in the legend of Figure 12) model remains slightly superior.

As previously discussed, precisely estimating plasma density and temperature is particularly challenging. Both fluid models fail to predict the total electron temperature accurately. Notably, the only parameter for which the fluid model employing anomalous collisionality outperforms the data-driven friction force model is the peak plasma density. Nevertheless, it is interesting to analyze the electron pressure neT_e, reported in Figure 13. As one can see, when using the data-driven model (i.e., Fluid 2 in the legend of Figure 13), we have a significantly better estimation of the electron pressure, regardless of the choice of the parameters $(\alpha_B^{\text{ch}}, \alpha_B^{\text{pl}})$ in the fluid model using the anomalous frequency (i.e., Fluid 1 and Fluid 1*).

VI. CONCLUSIONS

In this work, we compare the results of PIC and fluid simulations. The chosen setup is one of Charoy's *et al.*[58], which allows having a quasi-steady state (i.e., without current oscillations) and a non-collisional transport. Initially, we discuss how the anomalous transport can be included in the fluid electron momentum equation, highlighting the role of the anomalous force density $\mathbf{R}_{ei}$. Subsequently, we discuss the approximation by Sagdeev and Galeev[36], which led to the concept of anomalous collision frequency.

Our analysis of PIC results demonstrates that the anomalous force density is appropriately accounted for in the electron momentum equation. Nevertheless, when testing the anomalous collision frequency approximation using PIC simulation data, we find that the anomalous collision frequency, ν_a, cannot be directly computed from PIC data. This emphasizes a fundamental limitation in deriving this parameter from first principles, as the rate of change of momentum due to the anomalous force is not proportional to the electron momentum itself.

Within the Sagdeev and Galeev approximation context, we performed a comparative analysis between a PIC simulation and a 1D fluid model incorporating an anomalous collision frequency, ν_a. We iteratively determined an empirical ν_a by matching the overall current, achieving good agreement between the PIC and fluid simulations on several parameters. While this approach demonstrates the feasibility of modeling anomalous transport, it remains based on an assumption that is not rigorously validated, thereby limiting its predictive robustness.

As an alternative, we proposed a data-driven approach to model the electron-ion momentum exchange term, $\mathbf{R}_{ei}$. By directly using PIC data in the fluid simulation, we achieve a good agreement between PIC and fluid results. This method enhances the accuracy of the fluid model by providing a more consistent representation of anomalous transport effects and offers a viable path toward improving fluid-based simulations. However, it is important to note that our model relies on PIC data. To enhance its generality, alternative methods for generating input data, such as statistical approaches or theoretical closures, should be explored.

Future research will focus on extending and refining the proposed modeling framework. Our goals include introducing a heat flux closure to capture higher-order effects and improve energy transport description, investigating theoretical closures for the anomalous force term to reduce dependence on PIC data, and extending the current model to incorporate neutral gas dynamics for more comprehensive simulations that account for charged-neutral collisions. Some recent

works[65,66] have shown that using more moments and refined closures for pressure tensor and heat flux allows for reproducing kinetic results via fluid simulations better.

Modeling electron anomalous transport remains a significant challenge in the community[2]. Our work provides insights into the commonly used approximations in fluid models and their limitations. These advancements aim to establish a more rigorous and predictive modeling framework for HTs' simulations, facilitating the testing of theoretical closures for anomalous transport in fluid models.

Appendix A: PIC simulation details

We report here the details about the PIC simulation's setup. The reader should refer to Charoy *et al.*[58] for all details and comments. The PIC simulation employs a time step of $\Delta t = 5 \times 10^{-12}$ s and a uniform cell size of $\Delta x = \Delta y = 5 \times 10^{-5}$ m. The computational domain consists of 500 cells in the axial direction and 256 cells in the azimuthal direction, corresponding to physical dimensions of $L_x = 2.5$ cm and $L_y = 1.28$ cm, respectively.

The initial state of the simulation includes 75 macroparticles per cell, representing a plasma with an initial density of $n_{p,\mathrm{ini}} = 5 \times 10^{16}$ m^{-3}. The discharge is driven by a voltage of $U_0 = 200$ V. The initial electron temperature is set to $T_{e,\mathrm{ini}} = 10$ eV, while the ion temperature is initialized at $T_{i,\mathrm{ini}} = 0.5$ eV.

The axial profile of the radial magnetic field is imposed with a Gaussian shape, which reads

$$B(x) = a_k \exp\left(-\frac{(x - x_{B_{\max}})^2}{2\sigma_k^2}\right) + b_k \tag{A1}$$

with $k = 1$ for $x < x_{B_{\max}}$ and $k = 2$ for $x > x_{B_{\max}}$. The values of the coefficients a_k and b_k depend on:

$$B_0 = B(x = 0) = 6 \text{ mT}, \quad B_{L_x} = B(x = L_x) = 1 \text{ mT}, \quad B_{\max} = 10 \text{ mT},$$

$$x_{B_{\max}} = 0.3 L_x = 0.75 \text{ cm}, \quad \sigma_1 = \sigma_2 = 0.25 L_x = 0.625 \text{ cm},$$

with

$$\begin{cases} a_1 = \dfrac{B_m - B_0}{1 - \exp\left(-\frac{1}{2}\left(\frac{x_{B\max}}{\sigma_1}\right)^2\right)} \\ a_2 = \dfrac{B_m - B_{L_x}}{1 - \exp\left(-\frac{1}{2}\left(\frac{L_x - x_{B\max}}{\sigma_2}\right)^2\right)} \\ b_1 = B_0 - \dfrac{B_m \cdot \exp\left(-\frac{1}{2}\left(\frac{x_{B\max}}{\sigma_1}\right)^2\right)}{1 - \exp\left(-\frac{1}{2}\left(\frac{x_{B\max}}{\sigma_1}\right)^2\right)} \\ b_2 = B_{L_x} - \dfrac{B_m \cdot \exp\left(-\frac{1}{2}\left(\frac{L_x - x_{B\max}}{\sigma_2}\right)^2\right)}{1 - \exp\left(-\frac{1}{2}\left(\frac{L_x - x_{B\max}}{\sigma_2}\right)^2\right)} \end{cases} \tag{A2}$$

The ionization rate $S(x)$ depends only on x and is uniform in the azimuthal direction. It reads

$$S(x) = \begin{cases} S_0 \cos\left(\pi \frac{x - x_m}{x_2 - x_1}\right) & \text{for } x_1 \le x \le x_2 \\ 0 & \text{for } x < x_1 \text{ or } x > x_2 \end{cases} \tag{A3}$$

with $x_1 = 0.25$ cm, $x_2 = 1$ cm, $x_m = \frac{x_1 + x_2}{2} = 0.625$ cm, and $S_0 = 5.23 \times 10^{23}\,\mathrm{m^{-3}s^{-1}}$.

Appendix B: Fluid simulation details

The system of equations is solved using a finite volume scheme, with numerical fluxes at the cell interfaces computed using a Rusanov scheme. We used the method of lines to decouple space and time integration. The ODEs are solved with a Forward Euler scheme. We used 200 points in the axial direction, corresponding to a spatial timestep $\Delta x = 1.25 \times 10^{-4}$ m. We used an adaptive timestep Δt, issued by an imposed CFL = 0.01. With these conditions, a typical run requires about 1 minute on a single core. No particular optimization of the computational time has been adopted.

ACKNOWLEDGMENTS

The work of FP was partially supported by Agence de l'Innovation de Defense – AID - via Centre Interdisciplinaire d'Etudes pour la Défense et la Sécurité – CIEDS - (project 2023 – valid-HETion). This project was provided with computer and storage resources by GENCI at TGCC,

thanks to the grants 2024-A0160510439 and 2025-A0180510439 on the supercomputer Joliot Curie's Irene-ROME partition. The authors are grateful to Trevor Lafleur, Benjamin Esteves, Tsanko V. Tsankov, and all members of the COMHET project for their valuable insights.

DATA AVAILABILITY

The data that support the findings of this study are available from the corresponding author upon reasonable request.

Anomalous frequency study

REFERENCES

[1]D. M. Goebel and I. Katz, Fundamentals of Electric Propulsion: Ion and Hall Thrusters, JPL space science and technology series (Wiley, 2008).

[2]I. D. Kaganovich, A. Smolyakov, Y. Raitses, E. Ahedo, I. G. Mikellides, B. Jorns, F. Taccogna, R. Gueroult, S. Tsikata, A. Bourdon, J.-P. Boeuf, M. Keidar, A. T. Powis, M. Merino, M. Cappelli, K. Hara, J. A. Carlsson, N. J. Fisch, P. Chabert, I. Schweigert, T. Lafleur, K. Matyash, A. V. Khrabrov, R. W. Boswell, and A. Fruchtman, "Physics of E × B discharges relevant to plasma propulsion and similar technologies," Physics of Plasmas **27**, 120601 (2020).

[3]C. Birdsall, "Particle-in-cell charged-particle simulations, plus Monte Carlo collisions with neutral atoms, PIC-MCC," IEEE Transactions on Plasma Science **19**, 65–85 (1991).

[4]J.-P. Boeuf, "Tutorial: Physics and modeling of Hall thrusters," Journal of Applied Physics **121**, 011101 (2017).

[5]E. Ahedo, P. Martínez-Cerezo, and M. Martínez-Sánchez, "One-dimensional model of the plasma flow in a hall thruster," Physics of Plasmas **8**, 3058–3068 (2001).

[6]A. Cohen-Zur, A. Fruchtman, J. Ashkenazy, and A. Gany, "Analysis of the steady-state axial flow in the hall thruster," Physics of Plasmas **9**, 4363–4374 (2002).

[7]E. Bello-Benítez and E. Ahedo, "Stationary axial model of the Hall thruster plasma discharge: electron azimuthal inertia and far plume effects," Plasma Sources Science and Technology **32**, 115011 (2023).

[8]T. Lafleur and P. Chabert, "Analytical model of a hall thruster," Physics of Plasmas **31**, 093507 (2024).

[9]J. Boeuf and L. Garrigues, "Low frequency oscillations in a stationary plasma thruster," Journal of Applied Physics **84**, 3541–3554 (1998).

[10]J. Fife, M. Martinez-Sanchez, and J. Szabo, "A numerical study of low-frequency discharge oscillations in hall thrusters," in 33rd Joint Propulsion Conference and Exhibit (1997) p. 3052.

[11]F. Petronio, A. Alvarez Laguna, A. Bourdon, and P. Chabert, "Study of the breathing mode development in Hall thrusters using hybrid simulations," Journal of Applied Physics **135**, 073301 (2024), https://pubs.aip.org/aip/jap/article-pdf/doi/10.1063/5.0188859/19686444/073301_1_5.0188859.pdf.

[12]A. Morozov, "Wall conduction in a highly magnetized plasma," Journal of Applied Mechanics and Technical Physics **9**, 249–251 (1968).

[13]N. B. Meezan, W. A. Hargus Jr, and M. A. Cappelli, "Anomalous electron mobility in a coaxial hall discharge plasma," Physical Review E **63**, 026410 (2001).

[14]J. W. Koo and I. D. Boyd, "Modeling of anomalous electron mobility in Hall thrusters," Physics of Plasmas **13**, 033501 (2006).

[15]J. C. Adam, J. P. Boeuf, N. Dubuit, M. Dudeck, L. Garrigues, D. Gresillon, A. Heron, G. J. M. Hagelaar, V. Kulaev, N. Lemoine, S. Mazouffre, J. Perez Luna, V. Pisarev, and S. Tsikata, "Physics, simulation and diagnostics of Hall effect thrusters," Plasma Physics and Controlled Fusion **50**, 124041 (2008).

[16]L. Garrigues, J. Pérez-Luna, J. Lo, G. J. M. Hagelaar, J. P. Boeuf, and S. Mazouffre, "Empirical electron cross-field mobility in a hall effect thruster," Applied Physics Letters **95**, 141501 (2009), https://pubs.aip.org/aip/apl/article-pdf/doi/10.1063/1.3242336/14420417/141501_1_online.pdf.

[17]I. Katz, I. G. Mikellides, B. A. Jorns, and A. L. Ortega, "Hall2de simulations with an anomalous transport model based on the electron cyclotron drift instability," in 34nd International Electric Propulsion Conference, Vol. 402 (2015).

[18]V. N. Sokolsky, Konstantin E. Tsiolkovsky Selected Works (MIR publishers, 1968).

[19]E. Ahedo, J. M. Gallardo, and M. Martínez-Sánchez, "Effects of the radial plasma-wall interaction on the Hall thruster discharge," Physics of Plasmas **10**, 3397–3409 (2003).

[20]L. Garrigues, G. Hagelaar, C. Boniface, and J. Boeuf, "Anomalous conductivity and secondary electron emission in hall effect thrusters," Journal of applied physics **100**, 123301 (2006).

[21]A. Tavant, V. Croes, R. Lucken, T. Lafleur, A. Bourdon, and P. Chabert, "The effects of secondary electron emission on plasma sheath characteristics and electron transport in an E x B discharge via kinetic simulations," Plasma Sources Science and Technology **27**, 124001 (2018).

[22]D. Sydorenko, A. Smolyakov, I. Kaganovich, and Y. Raitses, "Kinetic simulation of secondary electron emission effects in Hall thrusters," Physics of Plasmas **13**, 014501 (2006).

[23]A. Smirnov, Y. Raitses, and N. J. Fisch, "Experimental and theoretical studies of cylindrical Hall thruster," Phys. Plasmas (2007), 10.1063/1.2718522.

[24]D. Sydorenko, A. Smolyakov, I. Kaganovich, and Y. Raitses, "Plasma-sheath instability in hall thrusters due to periodic modulation of the energy of secondary electrons in cyclotron motion," Physics of Plasmas **15**, 053506 (2008).

[25]G. Janes and R. Lowder, "Anomalous electron diffusion and ion acceleration in a low-density plasma," The Physics of Fluids **9**, 1115–1123 (1966).

[26]D. Forslund, R. Morse, and C. Nielson, "Electron cyclotron drift instability," Physical Review Letters **25**, 1266 (1970).

[27]J. C. Adam, A. Héron, and G. Laval, "Study of stationary plasma thrusters using two-dimensional fully kinetic simulations," Phys. Plasmas **11**, 12 (2004).

[28]A. Ducrocq, J. C. Adam, A. Héron, and G. Laval, "High-frequency electron drift instability in the cross-field configuration of Hall thrusters," Physics of Plasmas **13**, 102111 (2006).

[29]P. Coche and L. Garrigues, "A two-dimensional (azimuthal-axial) particle-in-cell model of a Hall thruster," Physics of Plasmas **21**, 023503 (2014).

[30]T. Lafleur, S. D. Baalrud, and P. Chabert, "Theory for the anomalous electron transport in Hall effect thrusters. I. Insights from particle-in-cell simulations," Physics of Plasmas **23**, 053502 (2016).

[31]T. Lafleur, S. D. Baalrud, and P. Chabert, "Theory for the anomalous electron transport in Hall effect thrusters. II. Kinetic model," Physics of Plasmas **23**, 053503 (2016).

[32]T. Lafleur and P. Chabert, "The role of instability-enhanced friction on 'anomalous' electron and ion transport in Hall-effect thrusters," Plasma Sources Science and Technology **27**, 015003 (2017).

[33]T. Lafleur, S. D. Baalrud, and P. Chabert, "Characteristics and transport effects of the electron drift instability in Hall-effect thrusters," Plasma Sources Science and Technology **26**, 024008 (2017).

[34]T. Lafleur, R. Martorelli, P. Chabert, and A. Bourdon, "Anomalous electron transport in Hall-effect thrusters: Comparison between quasi-linear kinetic theory and particle-in-cell simulations," Physics of Plasmas **25**, 061202 (2018).

[35]R. Martorelli, T. Lafleur, A. Bourdon, and P. Chabert, "Comparison between ad-hoc and instability-induced electron anomalous transport in a 1d fluid simulation of hall-effect thruster," Physics of Plasmas **26**, 083502 (2019).

[36]Sagdeev and Galeev, Nonlinear plasma physics (W. A. Benjamin Inc., 1969).

[37]G. J. M. Hagelaar, J. Bareilles, L. Garrigues, and J.-P. Boeuf, "Role of anomalous electron transport in a stationary plasma thruster simulation," Journal of Applied Physics **93**, 67–75 (2003).

[38]S. Barral, K. Makowski, Z. Peradzyński, N. Gascon, and M. Dudeck, "Wall material effects in stationary plasma thrusters. II. Near-wall and in-wall conductivity," Physics of Plasmas **10**, 4137–4152 (2003).

[39]M. Keidar, I. D. Boyd, and I. I. Beilis, "Modeling of a high-power thruster with anode layer," Physics of plasmas **11**, 1715–1722 (2004).

[40]S. Barral and E. Ahedo, "Low-frequency model of breathing oscillations in Hall discharges," Physical Review E **79**, 046401 (2009).

[41]K. Kwon, M. L. R. Walker, and D. N. Mavris, "Self-consistent, one-dimensional analysis of the Hall effect thruster," Plasma Sources Science and Technology **20**, 045021 (2011).

[42]I. G. Mikellides and I. Katz, "Numerical simulations of Hall-effect plasma accelerators on a magnetic-field-aligned mesh," Physical Review E **86**, 046703 (2012).

[43]I. G. Mikellides, B. Jorns, I. Katz, and A. Lopez Ortega, "Hall2de simulations with a first-principles electron transport model based on the electron cyclotron drift instability," in 52nd AIAA/SAE/ASEE Joint Propulsion Conference (2016) p. 4618.

[44]K. Hara and K. Hanquist, "Test cases for grid-based direct kinetic modeling of plasma flows," Plasma Sources Science and Technology **27**, 065004 (2018).

[45]T. Andreussi, V. Giannetti, A. Leporini, M. M. Saravia, and M. Andrenucci, "Influence of the magnetic field configuration on the plasma flow in Hall thrusters," Plasma Physics and Controlled Fusion **60**, 014015 (2018).

[46]A. Lopez Ortega, I. G. Mikellides, M. J. Sekerak, and B. A. Jorns, "Plasma simulations in 2-D (r-z) geometry for the assessment of pole erosion in a magnetically shielded Hall thruster," Journal of Applied Physics **125**, 033302 (2019).

[47]I. G. Mikellides and A. Lopez Ortega, "Challenges in the development and verification of first-principles models in Hall-effect thruster simulations that are based on anomalous resistivity and generalized Ohm's law," Plasma Sources Science and Technology **28**, 014003 (2019).

[48]V. Giannetti, M. M. Saravia, L. Leporini, S. Camarri, and T. Andreussi, "Numerical and Experimental Investigation of Longitudinal Oscillations in Hall Thrusters," Aerospace **8**, 148 (2021).

[49]K. Kwon, "Analytical modeling of the anomalous electron collision frequency in partially magnetized $E \times B$ plasmas," AIP Advances **11**, 085324 (2021).

[50]S. Camarri, V. Giannetti, M. M. Saravia, F. Califano, L. Leporini, and T. Andreussi, "On the onset of breathing mode in Hall thrusters and the role of electron mobility fluctuations," Frontiers in Physics **10**, 951960 (2022).

[51]D. Poli, E. Bello-Benítez, P. Fajardo, and E. Ahedo, "Time-dependent axial fluid model of the Hall thruster discharge and its plume," Journal of Physics D: Applied Physics **56**, 415203 (2023).

[52]A. Marín-Cebrián, E. Bello-Benítez, A. Domínguez-Vázquez, and E. Ahedo, "Non-Maxwellian electron effects on the macroscopic response of a Hall thruster discharge from an axial–radial kinetic model," Plasma Sources Science and Technology **33**, 025008 (2024).

[53]D. Poli, P. Fajardo, and E. Ahedo, "A non-neutral 1d fluid model of hall thruster discharges: full electron inertia and anode sheath reversal," Plasma Sources Science and Technology **33**, 075014 (2024).

[54]I. G. Mikellides, A. Lopez Ortega, and V. H. Chaplin, "Theory of the anomalous momentum exchange from wave–particle interactions in hall-effect ion accelerators and comparisons with measurements," Physics of Fluids **36**, 074121 (2024), https://pubs.aip.org/aip/pof/article-pdf/doi/10.1063/5.0213605/20081115/074121_1_5.0213605.pdf.

[55]T. A. Marks and B. A. Jorns, "Evaluation of algebraic models of anomalous transport in a multi-fluid Hall thruster code," Journal of Applied Physics **134**, 153301 (2023).

[56]T. Marks and A. Gorodetsky, "Hall thruster simulations in warpx," in IEPC Toulouse (2024).

[57]T. Lafleur, P. Chabert, M. M. Turner, and J. P. Booth, ""anomalous" collisionality in low-pressure plasmas," Physics of Plasmas **20**, 124503 (2013).

[58]T. Charoy, J. P. Boeuf, A. Bourdon, J. A. Carlsson, P. Chabert, B. Cuenot, D. Eremin, L. Garrigues, K. Hara, I. D. Kaganovich, A. T. Powis, A. Smolyakov, D. Sydorenko, A. Tavant, O. Vermorel, and W. Villafana, "2D axial-azimuthal particle-in-cell benchmark for low-temperature partially magnetized plasmas," Plasma Sources Science and Technology **28**, 105010 (2019).

[59]E. Ahedo, J. M. Gallardo, and M. Martínez-Sánchez, "Model of the plasma discharge in a Hall thruster with heat conduction," Physics of Plasmas **9**, 4061–4070 (2002), publisher: AIP Publishing.

[60]M. K. Scharfe, N. Gascon, M. A. Cappelli, and E. Fernandez, "Comparison of hybrid Hall thruster model to experimental measurements," Physics of Plasmas **13**, 083505 (2006).

[61]J. P. Boeuf and L. Garrigues, "E × B electron drift instability in Hall thrusters: Particle-in-cell simulations vs. theory," Physics of Plasmas **25**, 061204 (2018).

[62]W. Villafana, F. Petronio, A. C. Denig, M. J. Jimenez, D. Eremin, L. Garrigues, F. Taccogna, A. Alvarez-Laguna, J. P. Boeuf, A. Bourdon, P. Chabert, T. Charoy, B. Cuenot, K. Hara, F. Pechereau, A. Smolyakov, D. Sydorenko, A. Tavant, and O. Vermorel, "2D radial-azimuthal particle-in-cell benchmark for E × B discharges," Plasma Sources Science and Technology **30**, 075002 (2021).

Anomalous frequency study

[63]P. Parodi and F. Petronio, "Step-by-step verification of particle-in-cell monte-carlo collision codes," Physics of Plasmas (2025).

[64]T. Charoy, T. Lafleur, A. Tavant, P. Chabert, and A. Bourdon, "A comparison between kinetic theory and particle-in-cell simulations of anomalous electron transport in E × B plasma discharges," Physics of Plasmas **27**, 063510 (2020).

[65]Y. Yamashita, R. Lau, and K. Hara, "Inertial and anisotropic pressure effects on cross-field electron transport in low-temperature magnetized plasmas," Journal of Physics D: Applied Physics **56**, 384003 (2023).

[66]D. A. Kuldinow, Y. Yamashita, and K. Hara, "Ten-moment fluid model for low-temperature magnetized plasmas," Physics of Plasmas **31**, 123506 (2024).